Unstructured conservative level-set (UCLS) simulations of film boiling heat transfer ⋆

Néstor Balcázar-Arciniega[1][0000−0003−0776−2086], Joaquim Rigola[1][0000−0002−6685−3677], and Assensi Oliva[1][0000−0002−2805−4794]

[1] Heat and Mass Transfer Technological Centre, Universitat Politècnica de Catalunya-BarcelonaTech. Colom 11, 08222, Terrassa (Barcelona), Spain
nestor.balcazar@upc.edu, nestorbalcazar@yahoo.es

Abstract. A novel unstructured conservative level-set method for film boiling is introduced. The finite-volume discretization of transport equations is performed on collocated unstructured grids. Mass transfer is driven by thermal phase change and computed with the temperature gradient in the liquid and vapour phases at the interface. The fractional-step projection method is used for solving the pressure-velocity coupling. The convective term of transport equations is discretized by unstructured flux-limiter schemes to avoid numerical oscillations around the interface and minimize numerical diffusion. The central difference scheme discretizes diffusive terms. Verification and validation for film boiling on a flat surface are performed.

Keywords: Unstructured Conservative Level-Set Method · Unstructured Flux-Limiters · Finite-Volume Method · Unstructured Meshes · Vapor-Liquid Phase Change · Film Boiling

1 Introduction

Liquid-vapour phase change, e.g., boiling and condensation, is frequent in nature and industrial applications. Multiple engineering devices, from steam generators to cooling towers in nuclear and conventional thermal power plants, from unit operations to chemical reactors in the chemical processing industry, entail bubbles or droplets generated by liquid-vapour phase change, i.e., boiling, condensation and evaporation. Although empirical correlations have been proposed to perform predictions in boiling heat transfer, the interaction between fluid mechanics and transport phenomena in liquid-vapour phase change still needs to be better understood.

Research in Liquid-vapour phase change follows three paths: i) Experimental measurements with the appropriate visualization and instrumentation systems, ii) theoretical methods based on the analytical solutions of mathematical models with substantial

⋆ The main author, N. Balcázar-Arciniega, as a Serra-Húnter Lecturer (UPC-LE8027), acknowledges the Catalan Government for the financial support through this program. Computing time granted by the RES (IM-2023-1-0003, IM-2022-2-0009) is acknowledged. The authors acknowledge the financial support of the MINECO, Spain (PID2020-115837RB-100).

ICCS Camera Ready Version 2023
To cite this paper please use the final published version:
DOI: 10.1007/978-3-031-36030-5_26

simplifications of physics, and iii) numerical methods and their computational implementation. Complexities of liquid-vapour phase change constrain the analytical methods [1]. On the other hand, optical access can limit experimental measurements. Indeed, computational methods can often be the only mechanism to explore boiling heat transfer. Three computational methods are remarked: Euler-Euler method (E-E) or two-fluid model [47], Euler-Lagrange method (E-L) [47] and Direct Numerical Simulation (DNS) [47,68]. The E-E method formulates the continuous and dispersed phases as a fully interpenetrating continuum. The E-L method uses the Eulerian framework to solve the continuous phase, whereas the Lagrangian approach tracks the position and velocity of the fluid particles (bubbles or droplets). Finally, DNS solves all scales of fluid flow and interfaces without physics simplifications. Supercomputer advances have empowered the DNS as a practical approach for designing numerical experiments of liquid-vapour phase change.

Multiple methods have been reported for DNS of two-phase flows: front-tracking (FT) [70,65], level-set (LS) [45,61,26], Volume of Fluid (VoF) [32,50,68], coupled VoF-LS [60,59,11], and conservative level-set (CLS) [44,10,16], as examples. Further extensions of these methods include liquid-vapour phase change. For instance, [71,31,72,69,46,40] report VoF implementations of phase change. [55,56,57,58,51] propose extensions of LS methods to boiling heat transfer. Hybrid LS method and ghost-fluid approach [27] were reported by [28,42,63]. Coupled VoF-LS methods for phase change were reported by [43,64,53]. [34,23,24,67,33,48] inform a FT method for boiling. Although significant numerical and physical findings have been reported in previous efforts, most proposed methods employ structured and Cartesian meshes. Therefore, multiple flow conditions and engineering interest configurations must be explored. On the other hand, to the authors' knowledge, the robustness and accuracy of the unstructured conservative level-set (UCLS) method [16,14,10,8,18] to tackle film boiling heat transfer are still to be proven. Indeed, this work is a systematic step to develop numerical methods for complex interface physics in the framework of the UCLS method proposed by Balcazar et al. [16,14,10,8,18].

This research is organized as follows: Section 2 reviews the mathematical formulation. Section 2.4 presents the numerical methodology of the UCLS method on collocated unstructured meshes. Section 3 gives validations and numerical experiments of film boiling heat transfer. Finally, Section 4 report the conclusions.

2 Mathematical Formulation and Numerical Methods

2.1 Incompressible two-phase flow with phase change

The Navier-Stokes equations for the vapour phase (Ω_v) and liquid phase (Ω_l) are presented in the framework of the so-called one fluid formulation [66,47,68]:

$$\frac{\partial}{\partial t}(\rho \mathbf{v}) + \nabla \cdot (\rho \mathbf{v}\mathbf{v}) = -\nabla p + \nabla \cdot \mu \left(\nabla \mathbf{v}\right) + \nabla \cdot \mu (\nabla \mathbf{v})^T + (\rho - \rho_0)\mathbf{g} + \mathbf{f}_\sigma, \quad (1)$$

Here p is the pressure, $\mathbf{v}$ denotes the fluid velocity, μ refers to the dynamic viscosity, ρ refers to the fluid density, $\mathbf{g}$ is the gravity, $\mathbf{f}_\sigma$ denotes the surface tension force per

ICCS Camera Ready Version 2023
To cite this paper please use the final published version:
DOI: 10.1007/978-3-031-36030-5_26

unit volume, acting on the interface (Γ). If periodic boundary conditions are applied along the vertical axis (parallel to **g**), the acceleration of the flow field in the direction of **g** should be avoided. Accordingly Eq.(1) incorporates the force $-\rho_0\mathbf{g}$ [16,6,7], where $\rho_0 = V_\Omega^{-1}\int_\Omega (\rho_d H_d + \rho_c H_c)\, dV$. Otherwise, $\rho_0 = 0$.

Physical properties are constant at each fluid phase. Nevertheless, a jump discontinuity arises at the interface. Consequently, $\rho = \rho_l H_l + \rho_v H_v$, and $\mu = \mu_l H_l + \mu_v H_v$. Subscripts l and v refer to the liquid and vapour phases. H_v denotes the Heaviside step function, one in Ω_v and zero elsewhere. Moreover, $H_l = 1 - H_v$.

The mass conservation equation for the vapour phase and liquid phase are written as follows [8]:

$$\frac{\partial}{\partial t}H_v + \nabla\cdot(H_v\mathbf{v}) = \frac{\dot{m}_{lv}}{\rho_v}\delta_\Gamma,\ \frac{\partial}{\partial t}H_l + \nabla\cdot(H_l\mathbf{v}) = -\frac{\dot{m}_{lv}}{\rho_l}\delta_\Gamma, \tag{2}$$

where δ_Γ is the Dirac delta function concentrated at Γ, $\dot{m}_{lv}$ is the mass transfer rate promoted by the liquid-vapour phase change. As a consequence:

$$\nabla\cdot\mathbf{v} = \left(\frac{1}{\rho_v} - \frac{1}{\rho_l}\right)\dot{m}_{lv}\delta_\Gamma. \tag{3}$$

Eq.(3) poses an incompressible constraint in Ω, excluding the interface region (Γ).

2.2 Unstructured conservative level-set (UCLS) method

Interface capturing on collocated unstructured meshes is performed by the Unstructured Conservative Level-Set (UCLS) method proposed by Balcázar et al. [16][10]. An implicit function, $\phi = \frac{1}{2}\left(\tanh(\frac{d}{2\,\varepsilon}) + 1\right)$, represents the interface. Here, the parameter ε sets the interface thickness, and d is a signed distance function [45]. Furthermore, $\varepsilon_P = 0.5(h_P)^\alpha$ at the local cell Ω_P, h_P is the local grid size [16], $\alpha = 0.9$ unless otherwise stated. The Heaviside step function (H_l) introduced in Eq.(2) can be regularized by the UCLS function (ϕ). Therefore, $H_l^s = 1 - H_v^s = \phi$. And, consequently, Eq.(2) leads to an interface advection equation with phase change,

$$\frac{\partial\phi}{\partial t} + \nabla\cdot\phi\mathbf{v} = -\frac{1}{\rho_l}\dot{m}_{lv}\delta_\Gamma^s. \tag{4}$$

Here, $\delta_\Gamma^s = ||\nabla\phi||$ is the regularized Dirac delta function [16,10,15,8]. The UCLS profile is kept constant and sharp by solving the re-initialisation equation [10],

$$\frac{\partial\phi}{\partial\tau} + \nabla\cdot\phi(1-\phi)\mathbf{n}|_{\tau=0} = \nabla\cdot\varepsilon\nabla\phi, \tag{5}$$

where $\mathbf{n}|_{\tau=0}$ refers to the normal unit vector evaluated at $\tau = 0$. Eq.(5) is advanced in the pseudo-time (τ) upon arriving at the steady state. Interface curvature (κ) and normal unit vector (**n**) are computed as follows: $\mathbf{n}(\phi) = \nabla\phi_i\|\nabla\phi_i\|^{-1}$ and $\kappa(\phi) = -\nabla\cdot\mathbf{n}$. Furthermore, the Continuous Surface Force (CSF) model [20] is employed to compute the surface tension force in the framework of the UCLS method [16,14,9,18,10]. Consequently, $\mathbf{f}_\sigma = \sigma\kappa\mathbf{n}\delta_\Gamma^s = \sigma\kappa(\phi)\mathbf{n}(\phi)||\nabla\phi|| = \sigma\kappa(\phi)\nabla\phi$, where σ is the surface tension coefficient. Finally, the smoothed Heaviside step function (H_l^s and H_v^s) regularize physical properties. Indeed, $\mu = \mu_l H_l^s + \mu_v H_v^s$ and $\rho = \rho_l H_l^s + \rho_v H_v^s$. Consistently with Eq.(4), $H_l^s = \phi$ and $H_v^s = 1 - H_l^s$.

ICCS Camera Ready Version 2023
To cite this paper please use the final published version:
DOI: 10.1007/978-3-031-36030-5_26

2.3 Liquid-vapour phase change and energy equation

The following thermal energy equation computes the temperature on Ω_v:

$$\frac{\partial T}{\partial t} + \nabla \cdot (\mathbf{v}T) = \frac{1}{\rho c_p} \nabla \cdot (\lambda \nabla T), \tag{6}$$

where $c_p = c_{p,v}$ is the specific heat capacity at constant pressure, $\lambda = \lambda_v$ is the thermal conductivity, and $\rho = \rho_v$ is the density of the vapour phase. The vapour-liquid interface is at the saturation temperature (T_{sat}) [54], $T(\mathbf{x}, t) = T_{sat}$ on Ω_l. The mass transfer ($\dot{m}_{lv}$) driven by the liquid-vapour phase change is computed on the interface [8]: $\dot{m}_{lv} = h_{lv}^{-1} \ (\lambda_v (\nabla T \cdot \mathbf{n})_v - \lambda_l (\nabla T \cdot \mathbf{n})_l)$. Here, h_{lv} refers to the heat of vaporization. On the other hand, $T(\mathbf{x}, t) = T_{sat}$ in Ω_l implies that $(\nabla T \cdot \mathbf{n})_l = 0$. Finally, $(\nabla T \cdot \mathbf{n})_v = \Theta_{n,v}$ is extended on $\phi_{cut} < \phi < 1$, by solving a transport equation proposed in the framework of the UCLS method by [8]: $\frac{\partial}{\partial \tau} \Theta_{n,v} + \mathbf{n} \cdot \nabla \Theta_{n,v} = 0$. In this research $\phi_{cut} = 0.3$.

2.4 Finite-volume method: Unstructured flux-limiters

The finite-volume method discretizes transport equations for 3D collocated unstructured meshes [16]. The convective term of energy equation (Eq.(6)), level-set advection equation (Eq.(4)), and momentum transport equation (Eq.(1)), is explicitly computed through unstructured flux-limiter schemes proposed by Balcazar et al. [16,10]. Accordingly, the convective term in the local cell Ω_P is discretized as follows: $(\nabla \cdot \beta \psi \mathbf{v})_P = V_P^{-1} \sum_f \beta_f \psi_f (\mathbf{v}_f \cdot \mathbf{A}_f)$. Here, $\mathbf{A}_f = ||\mathbf{A}_f|| \mathbf{e}_f$ is the area vector. The unit vector $\mathbf{e}_f$, perpendicular to the face f, points outside the local cell Ω_P, V_P is the volume of Ω_P, and sub-index f refers to the cell faces. On the other hand,

$$\psi_f = \psi_{C_p} + \frac{1}{2} \mathrm{L}(\theta_f)(\psi_{D_p} - \psi_{C_p}), \tag{7}$$

where $\theta_f = (\psi_{C_p} - \psi_{U_p})/(\psi_{D_p} - \psi_{C_p})$ is a monitor variable, and $L(\theta_f)$ is the flux limiter function. Consistently with [16,10], subindex C_p refers to the upwind point, subindex U_p denotes the far-upwind point, and subindex D_p denotes the downwind point. Multiple flux limiters functions are implemented [62,25,38,39,41]:

$$L(\theta_f) \equiv \begin{cases} \max\{0, \min\{2\theta_f, 1\}, \min\{2, \theta_f\}\} & \text{SUPERBEE,} \\ (\theta_f + |\theta_f|)/(1 + |\theta_f|) & \text{VANLEER,} \\ \max\{0, \min\{4\theta_f, 0.75 + 0.25\theta_f, 2\}\} & \text{SMART,} \\ 1 & \text{CD,} \\ 0 & \text{UPWIND.} \end{cases} \tag{8}$$

A SUPERBEE flux limiter unless otherwise stated. The compressive term (Eq. (5)) is discretized as proposed by [16]: $(\nabla \cdot \phi_i (1 - \phi_i) \mathbf{n}_i^0)_P = \frac{1}{V_P} \sum_f (\phi_i (1 - \phi_i))_f \mathbf{n}_{i,f}^0 \cdot \mathbf{A}_f$. Here, $(\phi_i (1 - \phi_i))_f$ and $\mathbf{n}_{i,f}^0$ are linearly interpolated. The central difference scheme discretizes the diffusive term of transport equations [16]. Linear interpolation (arithmetic or distance weighted) [16] approximates the cell-face values. The weighted least-squares method [16,18,8,10] evaluates the gradients in Ω_P. The pressure-velocity coupling is solved by the fractional-step method [21,47,68,39]. First, a predictor velocity

ICCS Camera Ready Version 2023
To cite this paper please use the final published version:
DOI: 10.1007/978-3-031-36030-5_26

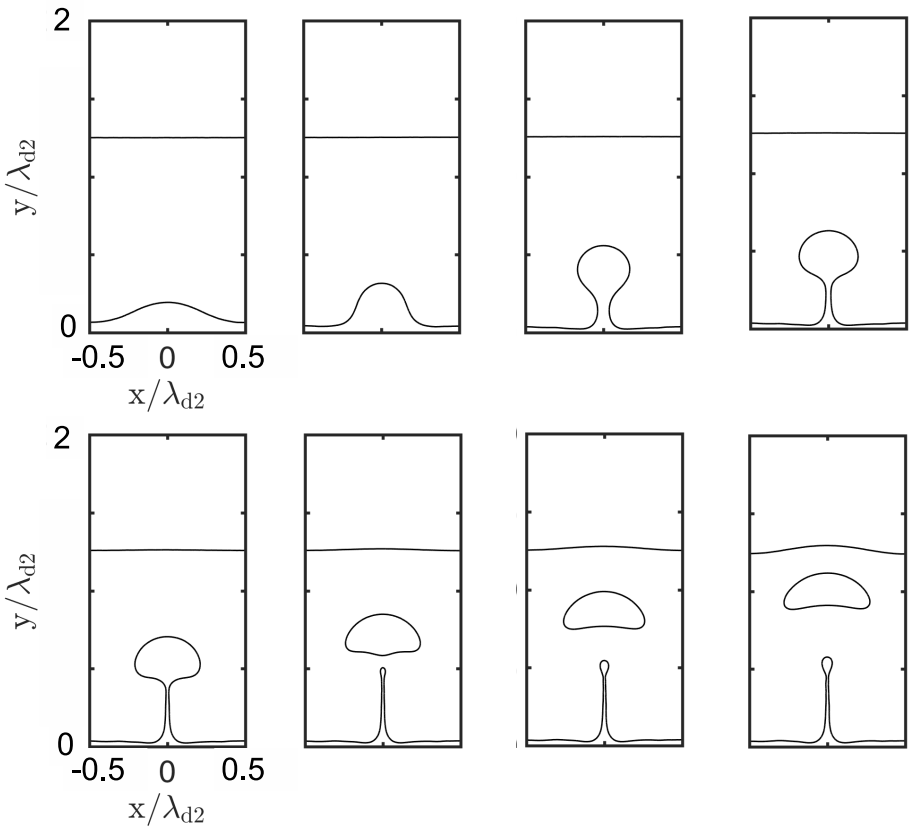

Fig. 1. Evolution of the liquid-vapour interface during film boiling. The dimensionless numbers are Gr $= 17.85$, Pr $= 4.2$ and Ja $= 0.064$. Physical properties ratios are $\mu_v/\mu_l = 0.386$, $\rho_v/\rho_l = 0.209$, $\lambda_v/\lambda_l = 0.281$, and $c_{p,v}/c_{p,l} = 1.830$. The grid size is $h = \lambda_{d2}300^{-1}$. $t^* = t/t_s = \{1.02, 3.06, 5.09, 6.11, 7.13, 8.15, 9.17, 10.19\}$.

($\mathbf{v}_P^*$) is calculated:

$$\frac{\rho_P \mathbf{v}_P^* - \rho_P^0 \mathbf{v}_P^0}{\Delta t} = \mathbf{C}_{\mathbf{v},P}^0 + \mathbf{D}_{\mathbf{v},P}^0 + (\rho_P - \rho_0)\mathbf{g} + \sigma\kappa_P(\nabla\phi)_P, \tag{9}$$

where $\mathbf{C_v} = -\nabla\cdot(\rho\mathbf{vv})$ and $\mathbf{D_v} = \nabla\cdot\mu\nabla\mathbf{v} + \nabla\cdot\mu(\nabla\mathbf{v})^T$. The superindex 0 refers to the previous time step. The incompressibility constraint with phase change (Eq.(3)) is applied to the corrector-step (Eq.(11)). Consequently, the following Poisson equation for the pressure arises:

$$\left(\nabla\cdot\frac{\Delta t}{\rho}\nabla p\right)_P = (\nabla\cdot\mathbf{v}^*)_P - \left(\frac{1}{\rho_v} - \frac{1}{\rho_l}\right)\dot{m}_{lv,P}\delta^s_{\Gamma,P},\ \mathbf{e}_{\partial\Omega}\cdot\nabla p|_{\partial\Omega} = 0. \tag{10}$$

ICCS Camera Ready Version 2023
To cite this paper please use the final published version:
DOI: 10.1007/978-3-031-36030-5_26

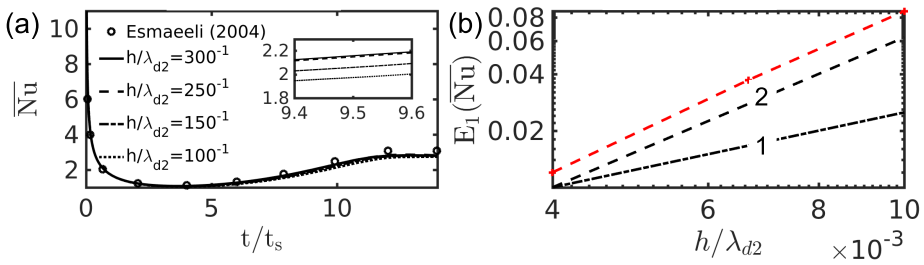

Fig. 2. Grid refinement test: (a) Time evolution of Nusselt number ($\overline{\mathrm{Nu}}$). The dimensionless numbers are Gr $= 17.85$, Pr $= 4.2$ and Ja $= 0.064$. Physical properties ratios are $\mu_v/\mu_l = 0.386$, $\rho_v/\rho_l = 0.209$, $\lambda_v/\lambda_l = 0.281$, and $c_{p,v}/c_{p,l} = 1.830$. Benchmark results extracted from Esmaeeli and Tryggvason (2004) [23] (symbols). (b) Order of convergence: The red line denotes present simulations. Black lines for first-order (1) and second-order (2) convergence. $E_1(\overline{\mathrm{Nu}}) = N^{-1}\sum_{i=1}^{N} ||\overline{\mathrm{Nu}}_i - \overline{\mathrm{Nu}}_{i,ref}||$, $\overline{\mathrm{Nu}}_{i,ref}$ refers to numerical results for the finest mesh, N is the number of sample points $(t_i t_s^{-1}, \overline{\mathrm{Nu}}_i)$.

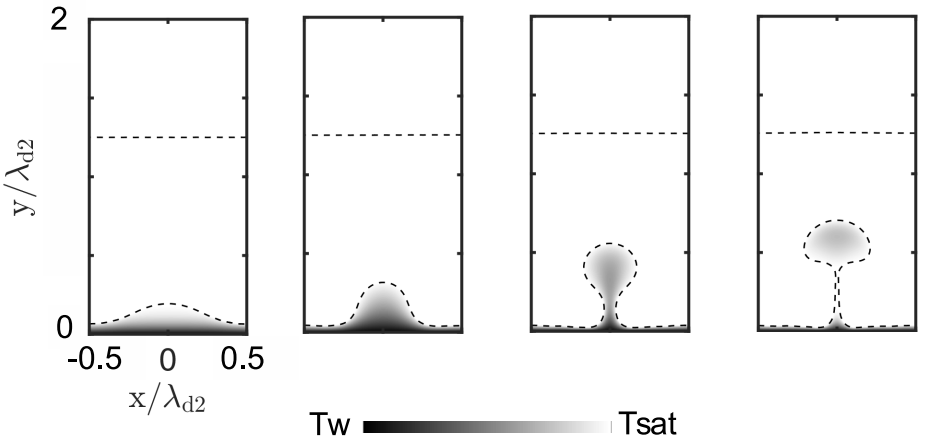

Fig. 3. Evolution of the liquid-vapour interface and temperature field during film boiling. Here, Pr $= 4.2$, Gr $= 17.85$, and Ja $= 0.064$. The ratio of thermophysical properties are $\rho_v/\rho_l = 0.209$, $\mu_v/\mu_l = 0.386$, $\lambda_v/\lambda_l = 0.281$, and $c_{p,v}/c_{p,l} = 1.830$. The grid size is $h = \lambda_{d2} 300^{-1}$.

Eq. (10) lead to a linear system, which is solved by the preconditioned conjugate gradient method [35]. In a further step, a corrected velocity ($\mathbf{v}_P$) is computed:

$$\frac{\rho_P \mathbf{v}_P - \rho_P \mathbf{v}_P^*}{\Delta t} = -\left(\nabla p\right)_P , \tag{11}$$

Furthermore, to avoid pressure-velocity decoupling on collocated meshes [49] and to fulfil the incompressibility constraint, a cell-face velocity $\mathbf{v}_f$ is interpolated (see [14]).

ICCS Camera Ready Version 2023
To cite this paper please use the final published version:
DOI: 10.1007/978-3-031-36030-5_26

The volume flux ($\mathbf{v}_f \cdot \mathbf{A}_f$), normal velocity ($\mathbf{v}_f \cdot \mathbf{e}_f$) or some equivalent variable are employed to solve the convective term of transport equations [14].

Technical details for the finite-volume discretization of the transport equations on 3D collocated unstructured meshes can be found in [16]. The new numerical methods for liquid-vapour phase change are developed in the framework of the UCLS solver proposed by Balcazar et al. [16]. The numerical code employs MPI (Message Passing Interface) for parallel communications and C++ for object-oriented design. The strong-speedup scalability is reported in [6,16].

3 Numerical Experiments

3.1 Validations and verifications of the UCLS method

The UCLS method was first introduced in [10]. A main contribution was the introduction of an accurate and original formulation of unstructured flux limiters for the finite-volume discretization of the level-set advection equation on collocated unstructured meshes. Systematic validations, verifications, and extensions of the UCLS method [10,16] include: thermocapillarity [14,4,18], gravity-driven rising bubbles [10,7,6,3,2], bubbly flows [12,6,16,17], binary droplet collision [12], collision of a droplet against a fluid-fluid interface [12], deformation of droplets [11], Taylor bubbles [29,30,2], falling droplets [9], atomization of gas-liquid jets [52], mass transfer in bubble swarms [16,17,5], and liquid-vapour phase change [8]. A comparison of the UCLS method [10] and coupled VoF-LS method [11] is reported in [9]. An extension of the UCLS method to tetrahedral adaptive mesh refinement has been reported in [3]. This research is a further step toward developing algorithms for complex interface physics in the framework of the UCLS method proposed by Balcazar et al. [16,18,13,7,12,10,15].

The following dimensionless numbers characterize the film boiling heat transfer:

$$\text{Gr} = \frac{\rho_v(\rho_l - \rho_v)||\mathbf{g}||X^3}{\mu_v^2}, \text{Pr} = \frac{\mu_v c_{p,v}}{\lambda_v}, \text{Ja} = \frac{c_{p,v}(T_w - T_{sat})}{h_{lv}}, \frac{\beta_v}{\beta_l}, \tag{12}$$

where Pr is the Prandtl number, Gr is the Grashof number, Ja denotes the Jakob number, $\beta = \{\rho, \mu, c_p, \lambda\}$. Here $X = l_s$ is a characteristic length scale. Furthermore, the computation of the Nusselt number (Nu) is performed as follows:

$$\begin{aligned} \text{Nu}(\mathbf{x}_w, t) &= \frac{X}{(T_w - T_{sat})}(\nabla T \cdot \mathbf{e}_w)(\mathbf{x}_w, t), \\ \overline{\text{Nu}}(t) &= \frac{1}{A_w}\int_{A_w} \text{Nu}(\mathbf{x}_w, t) dA, \\ \overline{\overline{\text{Nu}}} &= \frac{1}{T}\int_0^T \overline{\text{Nu}}(t) dt, \end{aligned} \tag{13}$$

where $\text{Nu}(\mathbf{x}_w, t)$ is the local Nusselt number. The unit vector $\mathbf{e}_w$, perpendicular to the bottom wall, points toward the fluids. $\overline{\text{Nu}}(t)$ refers to the space-averaged Nusselt number at the time t, A_w is the wall surface. $\overline{\overline{\text{Nu}}}$ denotes the time-averaged Nusselt number in the period T. On the other hand, $l_s = \left(\sigma||\mathbf{g}||^{-1}|\rho_l - \rho_v|^{-1}\right)^{1/2}$ is the capillary length

ICCS Camera Ready Version 2023
To cite this paper please use the final published version:
DOI: 10.1007/978-3-031-36030-5_26

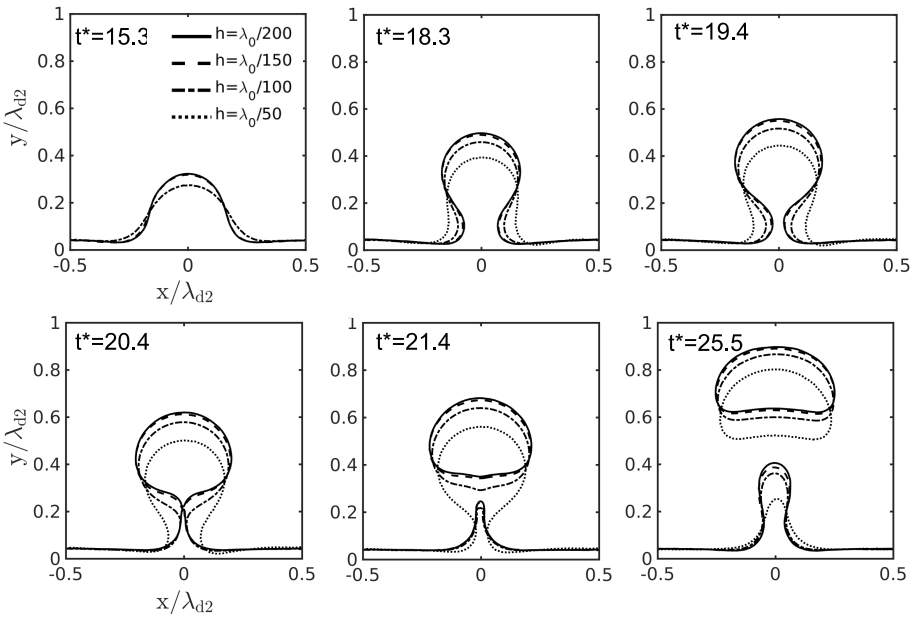

Fig. 4. Evolution of the liquid-vapour interface during film boiling. Here, Pr $= 1$, Gr $= 144.6$, and Ja $= 0.1$. The ratio of thermophysical properties are $\rho_v/\rho_l = 20^{-1}$, $\mu_v/\mu_l = 40^{-1}$, $\lambda_v/\lambda_l = 1$, and $c_{p,v}/c_{p,l} = 1$. The grid size is $h = \lambda_{d2}200^{-1}$.

scale, $v_s = (||\mathbf{g}||l_s)^{1/2}$ is the characteristic velocity, and $t_s = l_s/v_s$ is the characteristic time scale. The most dangerous wavelength [19] of Rayleigh-Taylor instability is defined as $\lambda_{d2} = 2\pi\sqrt{3}l_s$.

3.2 Film boiling on a horizontal plane

Ω is a rectangular domain $(L_x, L_y, L_z) = (\lambda_{d2}, 2\lambda_{d2}, h)$, discretized by triangular prisms with $h \approx \{\lambda_{d2}/150, \lambda_{d2}/200, \lambda_{d2}/250, \lambda_{d2}/300\}$. The initial film thickness is perturbed according to the interface shape: $y_\Gamma = y_0 + A\cos(2\pi x/\lambda_{d2})$ where $y_0 = 0.125\lambda_{d2}$, $A = 0.05\lambda_{d2}$ [23]. A vapour layer on top of the liquid layer is posed at $1.25\lambda_{d2}$. Neumann boundary conditions are set to all the boundaries except at the bottom wall. The no-slip boundary condition is applied for the bottom wall's velocity ($\mathbf{v}_w$). The temperature at the bottom wall is fixed to T_w. As initial conditions, the velocity field is zero, and the temperature field in Ω equals the saturation temperature T_{sat}. The computational setup is illustrated in Fig. 1.

A grid resolution test is depicted in Figure 2. The time evolution of the Nusselt number ($\overline{\text{Nu}}$) is shown in Figure 2a. The dimensionless numbers are Gr $= 17.85$, Pr $= 4.2$ and Ja $= 0.064$. Physical properties ratios are $\mu_v/\mu_l = 0.386$, $\rho_v/\rho_l = 0.209$, $\lambda_v/\lambda_l = 0.281$, and $c_{p,v}/c_{p,l} = 1.830$. Present results computed with the novel UCLS method for film boiling are in close agreement with front-tracking simulations reported

ICCS Camera Ready Version 2023
To cite this paper please use the final published version:
DOI: 10.1007/978-3-031-36030-5_26

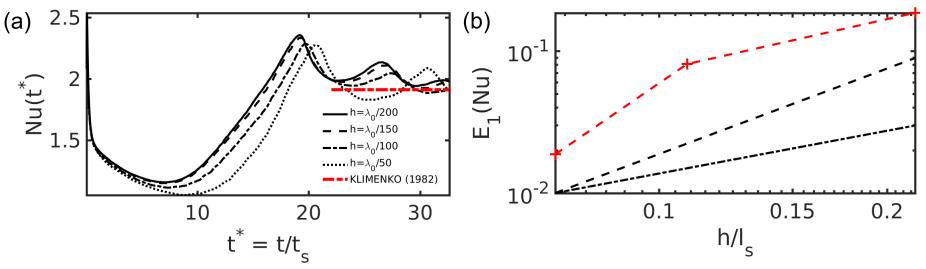

Fig. 5. Grid resolution test: (a) Time evolution of Nusselt number ($\overline{\text{Nu}}$). Here, Pr $= 1$, Gr $=$ 144.6, and Ja $= 0.1$. The ratio of thermophysical properties are $\rho_v/\rho_l = 20^{-1}$, $\mu_v/\mu_l = 40^{-1}$, $\lambda_v/\lambda_l = 1$, and $c_{p,v}/c_{p,l} = 1$. Numerical results are compared against Klimenko's correlation [36,37]. (b) Order of convergence: The red line denotes present simulations. Black lines for first-order (1) and second-order (2) convergence. $E_1(\overline{\text{Nu}}) = N^{-1}\sum_{i=1}^{N}||\overline{\text{Nu}}_i - \overline{\text{Nu}}_{i,ref}||$, $\overline{\text{Nu}}_{i,ref}$ refers to numerical results for the finest mesh, N is the number of sample points $(t_i t_s^{-1}, \overline{\text{Nu}}_i)$.

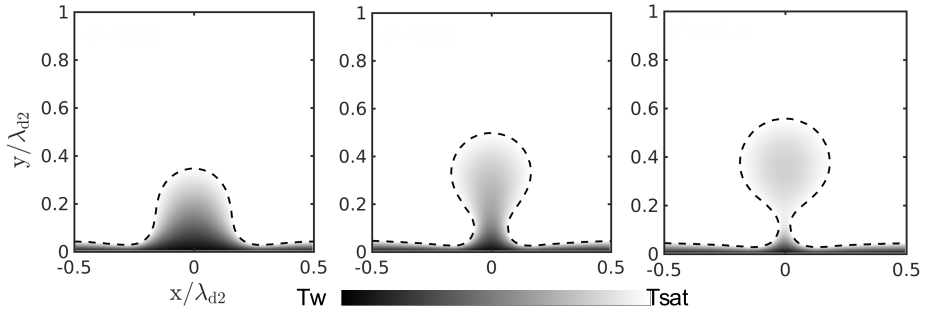

Fig. 6. Evolution of the liquid-vapour interface and temperature field during film boiling. Here, Pr $= 1$, Gr $= 144.6$, and Ja $= 0.1$. The ratio of thermophysical properties are $\rho_v/\rho_l = 20^{-1}$, $\mu_v/\mu_l = 40^{-1}$, $\lambda_v/\lambda_l = 1$, and $c_{p,v}/c_{p,l} = 1$. The grid size is $h = \lambda_{d2}200^{-1}$.

by Esmaeeli and Tryggvason (2004) [23]. Figure 2b shows that the UCLS method presents second-order convergence. The red line denotes present simulations. Black lines for first-order (1) and second-order (2) convergence. The error is computed as follows: $E_1(\overline{\text{Nu}}) = N^{-1}\sum_{i=1}^{N}||\overline{\text{Nu}}_i - \overline{\text{Nu}}_{i,ref}||$, $\overline{\text{Nu}}_{i,ref}$ refers to numerical results for the finest mesh, N is the number of sample points $(t_i t_s^{-1}, \overline{\text{Nu}}_i)$. The evolution of the liquid-vapour interface during film boiling is depicted in Figure 1, and the temperature field is shown in Figure 3.

A second case is performed on a rectangular domain $(L_x, L_y, L_z) = (\lambda_{d2}, \lambda_{d2}, h)$. Here, Pr $= 1$, Gr $= 144.6$, and Ja $= 0.1$. The ratio of thermophysical properties are $\rho_v/\rho_l = 20^{-1}$, $\mu_v/\mu_l = 40^{-1}$, $\lambda_v/\lambda_l = 1$, and $c_{p,v}/c_{p,l} = 1$. A test of grid convergence is illustrated in Figure 5, with $h \approx \{\lambda_{d2}/50, \lambda_{d2}/100, \lambda_{d2}/150, \lambda_{d2}/200\}$.

ICCS Camera Ready Version 2023
To cite this paper please use the final published version:
DOI: 10.1007/978-3-031-36030-5_26

The evolution of the liquid-vapour interface during film boiling is depicted in Figure 4, and the temperature field is shown in Figure 6.

4 CONCLUSIONS

- The UCLS method introduced by Balcazar et al.[17,16,18,10,12,7,12] has been extended for film boiling heat transfer. The numerical model has been verified and validated against numerical results of [22] and Klimenko's correlation [36,37].
- Unstructured flux-limiters schemes proposed by Balcazar et al. [10,16,11] for the discretization of the convective term, in the framework of the UCLS method, improves the numerical stability and minimize the numerical diffusion in simulations of film boiling heat transfer.
- Further verifications and validations, including three-dimensional cases, will be reported in a future work.

References

1. Alexiades, V., Solomon, A.D.: Mathematical Modeling of Melting and Freezing Processes. CRC Press, 1st edn. (1993). https://doi.org/10.1201/9780203749449, https://www.taylorfrancis.com/books/9781351433280
2. Antepara, O., Balczar, N., Oliva, A.: Tetrahedral adaptive mesh refinement for twophase flows using conservative levelset method. International Journal for Numerical Methods in Fluids **93**, 481–503 (2021). https://doi.org/10.1002/fld.4893, https://onlinelibrary.wiley.com/doi/10.1002/fld.4893
3. Antepara, O., Balczar, N., Rigola, J., Oliva, A.: Numerical study of rising bubbles with path instability using conservative level-set and adaptive mesh refinement. Computers and Fluids **187**, 83–97 (2019). https://doi.org/10.1016/j.compfluid.2019.04.013, https://linkinghub.elsevier.com/retrieve/pii/S0045793018306297
4. Balcazar, N., Antepara, O., Rigola, J., Oliva, A.: Dns of thermocapillary migration of deformable droplets. In: Salvetti M., Armenio V., Frhlich J., Geurts B., Kuerten H. (eds) Direct and Large-Eddy Simulation XI. ERCOFTAC Series. **25** (2019). https://doi.org/https://doi.org/10.1007/978-3-030-04915-7$_2$8
5. Balcazar, N., Antepara, O., Rigola, J., Oliva, A.: Dns of drag-force and reactive mass transfer in gravity-driven bubbly flows. In: Garca-Villalba, M., Kuerten, H., Salvetti, M. (eds) Direct and Large Eddy Simulation XII. DLES 2019. ERCOFTAC Series, vol 27. Springer, Cham pp. 119–125 (2020). https://doi.org/10.1007/978-3-030-42822-8$_1$6, http://link.springer.com/10.1007/978-3-030-42822-8_16
6. Balcazar, N., Castro, J., Rigola, J., Oliva, A.: Dns of the wall effect on the motion of bubble swarms. Procedia Computer Science **108**, 2008–2017 (2017). https://doi.org/10.1016/j.procs.2017.05.076, https://linkinghub.elsevier.com/retrieve/pii/S1877050917306142
7. Balcazar, N., Lehmkuhl, O., Jofre, L., Oliva, A.: Level-set simulations of buoyancy-driven motion of single and multiple bubbles. International Journal of Heat and Fluid Flow **56** (2015). https://doi.org/10.1016/j.ijheatfluidflow.2015.07.004
8. Balcazar, N., Rigola, J., Oliva, A.: Unstructured level-set method for saturated liquid-vapor phase change. In: WCCM-ECCOMAS 2020. Volume 600 - Fluid Dynamics and Transport Phenomena. pp. 1–12 (2021). https://doi.org/10.23967/wccm-eccomas.2020.352, https://www.scipedia.com/public/Balcazar_et_al_2021a

ICCS Camera Ready Version 2023
To cite this paper please use the final published version:
DOI: 10.1007/978-3-031-36030-5_26

9. Balcazar, N., Castro, J., Chiva, J., Oliva, A.: Dns of falling droplets in a vertical channel. International Journal of Computational Methods and Experimental Measurements **6**, 398–410 (11 2017). https://doi.org/10.2495/CMEM-V6-N2-398-410, http://www.witpress.com/doi/journals/CMEM-V6-N2-398-410
10. Balcazar, N., Jofre, L., Lehmkuhl, O., Castro, J., Rigola, J.: A finite-volume/level-set method for simulating two-phase flows on unstructured grids. International Journal of Multiphase Flow **64**, 55–72 (2014). https://doi.org/10.1016/j.ijmultiphaseflow.2014.04.008, https://linkinghub.elsevier.com/retrieve/pii/S030193221400072X
11. Balcazar, N., Lehmkuhl, O., Jofre, L., Rigola, J., Oliva, A.: A coupled volume-of-fluid/level-set method for simulation of two-phase flows on unstructured meshes. Computers and Fluids **124**, 12–29 (2016). https://doi.org/10.1016/j.compfluid.2015.10.005, https://linkinghub.elsevier.com/retrieve/pii/S0045793015003394
12. Balcazar, N., Lehmkuhl, O., Rigola, J., Oliva, A.: A multiple marker level-set method for simulation of deformable fluid particles. International Journal of Multiphase Flow **74**, 125–142 (2015). https://doi.org/10.1016/j.ijmultiphaseflow.2015.04.009
13. Balcazar, N., Oliva, A., Rigola, J.: A level-set method for thermal motion of bubbles and droplets. Journal of Physics: Conference Series **745**, 032113 (2016). https://doi.org/10.1088/1742-6596/745/3/032113
14. Balcazar, N., Rigola, J., Castro, J., Oliva, A.: A level-set model for thermocapillary motion of deformable fluid particles. International Journal of Heat and Fluid Flow **62**, 324–343 (12 2016). https://doi.org/10.1016/j.ijheatfluidflow.2016.09.015, https://linkinghub.elsevier.com/retrieve/pii/S0142727X16301266
15. Balcazar-Arciniega, N., Rigola, J., Oliva, A.: A level-set model for two-phase flow with variable surface tension: Thermocapillary and surfactants. 8th European Congress on Computational Methods in Applied Sciences and Engineering (2022). https://doi.org/10.23967/eccomas.2022.011, https://www.scipedia.com/public/Balcazar_Arciniega_et_al_2022a
16. Balcazar-Arciniega, N., Antepara, O., Rigola, J., Oliva, A.: A level-set model for mass transfer in bubbly flows. International Journal of Heat and Mass Transfer **138**, 335–356 (2019). https://doi.org/10.1016/j.ijheatmasstransfer.2019.04.008
17. Balcazar-Arciniega, N., Rigola, J., Oliva, A.: Dns of mass transfer from bubbles rising in a vertical channel. Lecture Notes in Computer Science (including subseries Lecture Notes in Artificial Intelligence and Lecture Notes in Bioinformatics) **11539 LNCS**, 596–610 (2019). https://doi.org/10.1007/978-3-030-22747-0$_45$, http://link.springer.com/10.1007/978-3-030-22747-0_45
18. Balcazar-Arciniega, N., Rigola, J., Oliva, A.: Dns ofmass transfer in bi-dispersed bubble swarms. In: Computational Science ICCS 2022. ICCS 2022. Lecture Notes in Computer Science, vol 13353. Springer, Cham **13353**, 284–296 (2022). https://doi.org/10.1007/978-3-031-08760-8$_24$, https://link.springer.com/10.1007/978-3-031-08760-8_24
19. Berenson, P.J.: Film-boiling heat transfer from a horizontal surface. Journal of Heat Transfer **83**, 351–356 (1961). https://doi.org/10.1115/1.3682280, https://asmedigitalcollection.asme.org/heattransfer/article/83/3/351/430783/FilmBoiling-Heat-Transfer-From-a-Horizontal
20. Brackbill, J.U., Kothe, D.B., Zemach, C.: A continuum method for modeling surface tension. Journal of Computational Physics **100**, 335–354 (1992). https://doi.org/10.1016/0021-9991(92)90240-Y, https://linkinghub.elsevier.com/retrieve/pii/002199919290240Y
21. Chorin, A.J.: Numerical solution of the navier-stokes equations. Mathematics of Computation **22**, 745 (1968). https://doi.org/10.2307/2004575, https://www.jstor.org/stable/2004575?origin=crossref

ICCS Camera Ready Version 2023
To cite this paper please use the final published version:
DOI: 10.1007/978-3-031-36030-5_26

22. Esmaeeli, A., Tryggvason, G.: Computations of explosive boiling in microgravity. Journal of Scientific Computing (2003). https://doi.org/10.1023/A:1025347823928
23. Esmaeeli, A., Tryggvason, G.: Computations of film boiling. part i: numerical method. International Journal of Heat and Mass Transfer **47**, 5451–5461 (2004). https://doi.org/10.1016/j.ijheatmasstransfer.2004.07.027, https://linkinghub.elsevier.com/retrieve/pii/S0017931004002947
24. Esmaeeli, A., Tryggvason, G.: A front tracking method for computations of boiling in complex geometries. International Journal of Multiphase Flow **30**, 1037–1050 (7 2004). https://doi.org/10.1016/j.ijmultiphaseflow.2004.04.008, https://linkinghub.elsevier.com/retrieve/pii/S0301932204000576
25. Gaskell, P.H., Lau, A.K.C.: Curvature-compensated convective transport: Smart, a new boundedness- preserving transport algorithm. International Journal for Numerical Methods in Fluids **8**, 617–641 (1988). https://doi.org/10.1002/fld.1650080602, http://doi.wiley.com/10.1002/fld.1650080602
26. Gibou, F., Fedkiw, R., Osher, S.: A review of level-set methods and some recent applications. Journal of Computational Physics **353**, 82–109 (1 2018). https://doi.org/10.1016/j.jcp.2017.10.006, https://linkinghub.elsevier.com/retrieve/pii/S0021999117307441
27. Gibou, F., Fedkiw, R.P., Cheng, L.T., Kang, M.: A second-order-accurate symmetric discretization of the poisson equation on irregular domains. Journal of Computational Physics **176**, 205–227 (2 2002). https://doi.org/10.1006/jcph.2001.6977, https://linkinghub.elsevier.com/retrieve/pii/S0021999101969773
28. Gibou, F., Chen, L., Nguyen, D., Banerjee, S.: A level set based sharp interface method for the multiphase incompressible navierstokes equations with phase change. Journal of Computational Physics **222**, 536–555 (3 2007). https://doi.org/10.1016/j.jcp.2006.07.035, https://linkinghub.elsevier.com/retrieve/pii/S0021999106003652
29. Gutirrez, E., Balczar, N., Bartrons, E., Rigola, J.: Numerical study of taylor bubbles rising in a stagnant liquid using a level-set/moving-mesh method. Chemical Engineering Science **164**, 158–177 (6 2017). https://doi.org/10.1016/j.ces.2017.02.018
30. Gutirrez, E., Favre, F., Balczar, N., Amani, A., Rigola, J.: Numerical approach to study bubbles and drops evolving through complex geometries by using a level set moving mesh immersed boundary method. Chemical Engineering Journal **349**, 662–682 (10 2018). https://doi.org/10.1016/j.cej.2018.05.110
31. Hardt, S., Wondra, F.: Evaporation model for interfacial flows based on a continuum-field representation of the source terms. Journal of Computational Physics **227**, 5871–5895 (5 2008). https://doi.org/10.1016/j.jcp.2008.02.020, https://linkinghub.elsevier.com/retrieve/pii/S0021999108001228
32. Hirt, C., Nichols, B.: Volume of fluid (vof) method for the dynamics of free boundaries. Journal of Computational Physics **39**, 201–225 (1 1981). https://doi.org/10.1016/0021-9991(81)90145-5, https://linkinghub.elsevier.com/retrieve/pii/0021999181901455
33. Irfan, M., Muradoglu, M.: A front tracking method for direct numerical simulation of evaporation process in a multiphase system. Journal of Computational Physics **337**, 132–153 (5 2017). https://doi.org/10.1016/j.jcp.2017.02.036, https://linkinghub.elsevier.com/retrieve/pii/S0021999117301304
34. Juric, D., Tryggvason, G.: Computations of boiling flows. International Journal of Multiphase Flow **24**, 387–410 (4 1998). https://doi.org/10.1016/S0301-9322(97)00050-5, https://linkinghub.elsevier.com/retrieve/pii/S0301932297000505

ICCS Camera Ready Version 2023
To cite this paper please use the final published version:
DOI: 10.1007/978-3-031-36030-5_26

35. Karniadakis, G.E., II, R.M.K.: Parallel Scientific Computing in C++ and MPI. Cambridge University Press (6 2003). https://doi.org/10.1017/CBO9780511812583, https://www.cambridge.org/core/product/identifier/9780511812583/type/book
36. Klimenko, V.: Film boiling on a horizontal plate new correlation. International Journal of Heat and Mass Transfer **24**, 69–79 (1 1981). https://doi.org/10.1016/0017-9310(81)90094-6
37. Klimenko, V., Shelepen, A.: Film boiling on a horizontal platea supplementary communication. International Journal of Heat and Mass Transfer **25**, 1611–1613 (10 1982). https://doi.org/10.1016/0017-9310(82)90042-4
38. LeVeque, R.J.: High-resolution conservative algorithms for advection in incompressible flow. SIAM Journal on Numerical Analysis **33**, 627–665 (4 1996). https://doi.org/10.1137/0733033
39. LeVeque, R.J.: Finite Volume Methods for Hyperbolic Problems. Cambridge University Press (8 2002). https://doi.org/10.1017/CBO9780511791253, https://www.cambridge.org/core/product/identifier/9780511791253/type/book
40. Ma, C., Bothe, D.: Numerical modeling of thermocapillary two-phase flows with evaporation using a two-scalar approach for heat transfer. Journal of Computational Physics **233**, 552–573 (1 2013). https://doi.org/10.1016/j.jcp.2012.09.011, https://linkinghub.elsevier.com/retrieve/pii/S0021999112005426
41. Moukalled, F., Mangani, L., Darwish, M.: The Finite Volume Method in Computational Fluid Dynamics. Springer (2016)
42. Ningegowda, B., Ge, Z., Lupo, G., Brandt, L., Duwig, C.: A mass-preserving interface-correction level set/ghost fluid method for modeling of three-dimensional boiling flows. International Journal of Heat and Mass Transfer **162**, 120382 (12 2020). https://doi.org/10.1016/j.ijheatmasstransfer.2020.120382, https://linkinghub.elsevier.com/retrieve/pii/S0017931020333184
43. Ningegowda, B., Premachandran, B.: A coupled level set and volume of fluid method with multi-directional advection algorithms for two-phase flows with and without phase change. International Journal of Heat and Mass Transfer **79**, 532–550 (12 2014). https://doi.org/10.1016/j.ijheatmasstransfer.2014.08.039, https://linkinghub.elsevier.com/retrieve/pii/S0017931014007261
44. Olsson, E., Kreiss, G.: A conservative level set method for two phase flow. Journal of Computational Physics **210**, 225–246 (11 2005). https://doi.org/10.1016/j.jcp.2005.04.007, https://linkinghub.elsevier.com/retrieve/pii/S0021999105002184
45. Osher, S., Sethian, J.A.: Fronts propagating with curvature-dependent speed: Algorithms based on hamilton-jacobi formulations. Journal of Computational Physics **79**, 12–49 (11 1988). https://doi.org/10.1016/0021-9991(88)90002-2, https://linkinghub.elsevier.com/retrieve/pii/0021999188900022
46. Perez-Raya, I., Kandlikar, S.G.: Discretization and implementation of a sharp interface model for interfacial heat and mass transfer during bubble growth. International Journal of Heat and Mass Transfer **116**, 30–49 (1 2018). https://doi.org/10.1016/j.ijheatmasstransfer.2017.08.106, https://linkinghub.elsevier.com/retrieve/pii/S0017931017322408
47. Prosperetti, A., Tryggvason, G.: Computational Methods for Multiphase Flow. Cambridge University Press (2007). https://doi.org/10.1017/CBO9780511607486
48. Rajkotwala, A., Panda, A., Peters, E., Baltussen, M., van der Geld, C., Kuerten, J., Kuipers, J.: A critical comparison of smooth and sharp interface methods for phase transition. International Journal of Multiphase Flow **120**, 103093 (11 2019). https://doi.org/10.1016/j.ijmultiphaseflow.2019.103093, https://linkinghub.elsevier.com/retrieve/pii/S0301932219301016

ICCS Camera Ready Version 2023
To cite this paper please use the final published version:
DOI: 10.1007/978-3-031-36030-5_26

49. Rhie, C.M., Chow, W.L.: Numerical study of the turbulent flow past an airfoil with trailing edge separation. AIAA Journal **21**, 1525–1532 (1983). https://doi.org/10.2514/3.8284, https://arc.aiaa.org/doi/10.2514/3.8284
50. Rider, W.J., Kothe, D.B.: Reconstructing volume tracking. Journal of Computational Physics **141**, 112–152 (4 1998). https://doi.org/10.1006/jcph.1998.5906, https://linkinghub.elsevier.com/retrieve/pii/S002199919895906X
51. Sato, Y., Nieno, B.: A sharp-interface phase change model for a mass-conservative interface tracking method. Journal of Computational Physics **249**, 127–161 (9 2013). https://doi.org/10.1016/j.jcp.2013.04.035, https://linkinghub.elsevier.com/retrieve/pii/S0021999113003197
52. Schillaci, E., Antepara, O., Balczar, N., Serrano, J.R., Oliva, A.: A numerical study of liquid atomization regimes by means of conservative level-set simulations. Computers and Fluids **179**, 137–149 (2019). https://doi.org/10.1016/j.compfluid.2018.10.017, https://linkinghub.elsevier.com/retrieve/pii/S0045793018307801
53. Singh, N.K., Premachandran, B.: A coupled level set and volume of fluid method on unstructured grids for the direct numerical simulations of two-phase flows including phase change. International Journal of Heat and Mass Transfer **122**, 182–203 (7 2018). https://doi.org/10.1016/j.ijheatmasstransfer.2018.01.091, https://linkinghub.elsevier.com/retrieve/pii/S0017931017341194
54. Son, G., Dhir, V.K.: Numerical simulation of saturated film boiling on a horizontal surface. Journal of Heat Transfer **119**, 525–533 (8 1997). https://doi.org/10.1115/1.2824132, https://asmedigitalcollection.asme.org/heattransfer/article/119/3/525/415631/Numerical-Simulation-of-Saturated-Film-Boiling-on
55. Son, G., Dhir, V.K.: Numerical simulation of film boiling near critical pressures with a level set method. Journal of Heat Transfer **120**, 183–192 (2 1998). https://doi.org/10.1115/1.2830042, https://asmedigitalcollection.asme.org/heattransfer/article/120/1/183/383014/Numerical-Simulation-of-Film-Boiling-Near-Critical
56. Son, G., Dhir, V.K., Ramanujapu, N.: Dynamics and heat transfer associated with a single bubble during nucleate boiling on a horizontal surface. Journal of Heat Transfer **121**, 623–631 (8 1999). https://doi.org/10.1115/1.2826025, https://asmedigitalcollection.asme.org/heattransfer/article/121/3/623/429987/Dynamics-and-Heat-Transfer-Associated-With-a
57. Son, G., Dhir, V.K.: Numerical simulation of nucleate boiling on a horizontal surface at high heat fluxes. International Journal of Heat and Mass Transfer **51**, 2566–2582 (5 2008). https://doi.org/10.1016/j.ijheatmasstransfer.2007.07.046, https://linkinghub.elsevier.com/retrieve/pii/S0017931007005212
58. Son, G., Dhir, V.K.: Three-dimensional simulation of saturated film boiling on a horizontal cylinder. International Journal of Heat and Mass Transfer **51**, 1156–1167 (3 2008). https://doi.org/10.1016/j.ijheatmasstransfer.2007.04.026, https://linkinghub.elsevier.com/retrieve/pii/S0017931007003304
59. Sun, D., Tao, W.: A coupled volume-of-fluid and level set (voset) method for computing incompressible two-phase flows. International Journal of Heat and Mass Transfer **53**, 645–655 (1 2010). https://doi.org/10.1016/j.ijheatmasstransfer.2009.10.030, https://linkinghub.elsevier.com/retrieve/pii/S0017931009005717
60. Sussman, M., Puckett, E.G.: A coupled level set and volume-of-fluid method for computing 3d and axisymmetric incompressible two-phase flows. Journal of Computational Physics **162**, 301–337 (8 2000). https://doi.org/10.1006/jcph.2000.6537, https://linkinghub.elsevier.com/retrieve/pii/S0021999100965379

ICCS Camera Ready Version 2023
To cite this paper please use the final published version:
DOI: 10.1007/978-3-031-36030-5_26

61. Sussman, M., Smereka, P., Osher, S.: A level set approach for computing solutions to incompressible two-phase flow. Journal of Computational Physics **114**, 146–159 (9 1994). https://doi.org/10.1006/jcph.1994.1155, https://linkinghub.elsevier.com/retrieve/pii/S0021999184711557
62. Sweby, P.K.: High resolution schemes using flux limiters for hyperbolic conservation laws. SIAM Journal on Numerical Analysis **21**, 995–1011 (10 1984). https://doi.org/10.1137/0721062, http://epubs.siam.org/doi/10.1137/0721062
63. Tanguy, S., Mnard, T., Berlemont, A.: A level set method for vaporizing two-phase flows. Journal of Computational Physics **221**, 837–853 (2 2007). https://doi.org/10.1016/j.jcp.2006.07.003, https://linkinghub.elsevier.com/retrieve/pii/S0021999106003214
64. Tomar, G., Biswas, G., Sharma, A., Welch, S.W.J.: Multimode analysis of bubble growth in saturated film boiling. Physics of Fluids **20**, 092101 (9 2008). https://doi.org/10.1063/1.2976764, http://aip.scitation.org/doi/10.1063/1.2976764
65. Tryggvason, G., Bunner, B., Esmaeeli, A., Juric, D., Al-Rawahi, N., Tauber, W., Han, J., Nas, S., Jan, Y.J.: A front-tracking method for the computations of multiphase flow. Journal of Computational Physics **169**, 708–759 (5 2001). https://doi.org/10.1006/jcph.2001.6726, https://linkinghub.elsevier.com/retrieve/pii/S0021999101967269
66. Tryggvason, G., Bunner, B., Esmaeeli, A., Juric, D., Al-Rawahi, N., Tauber, W., Han, J., Nas, S., Jan, Y.J.: A front-tracking method for the computations of multiphase flow. Journal of Computational Physics **169**, 708–759 (5 2001). https://doi.org/10.1006/jcph.2001.6726, https://linkinghub.elsevier.com/retrieve/pii/S0021999101967269
67. Tryggvason, G., Esmaeeli, A., Al-Rawahi, N.: Direct numerical simulations of flows with phase change. Computers and Structures **83**, 445–453 (2 2005). https://doi.org/10.1016/j.compstruc.2004.05.021, https://linkinghub.elsevier.com/retrieve/pii/S0045794904004158
68. Tryggvason, G., Scardovelli, R., Zaleski, S.: The volume-of-fluid method (1 2001). https://doi.org/10.1017/CBO9780511975264.006, https://www.cambridge.org/core/product/identifier/CBO9780511975264A041/type/book_part
69. Tsui, Y.Y., Lin, S.W.: Three-dimensional modeling of fluid dynamics and heat transfer for two-fluid or phase change flows. International Journal of Heat and Mass Transfer **93**, 337–348 (2 2016). https://doi.org/10.1016/j.ijheatmasstransfer.2015.09.021, https://linkinghub.elsevier.com/retrieve/pii/S0017931015009643
70. Unverdi, S.O., Tryggvason, G.: A front-tracking method for viscous, incompressible, multi-fluid flows. Journal of Computational Physics **100**, 25–37 (5 1992). https://doi.org/10.1016/0021-9991(92)90307-K, https://linkinghub.elsevier.com/retrieve/pii/002199919290307K
71. Welch, S.W., Wilson, J.: A volume of fluid based method for fluid flows with phase change. Journal of Computational Physics **160**, 662–682 (5 2000). https://doi.org/10.1006/jcph.2000.6481, https://linkinghub.elsevier.com/retrieve/pii/S0021999100964817
72. Yuan, M., Yang, Y., Li, T., Hu, Z.: Numerical simulation of film boiling on a sphere with a volume of fluid interface tracking method. International Journal of Heat and Mass Transfer **51**, 1646–1657 (4 2008). https://doi.org/10.1016/j.ijheatmasstransfer.2007.07.037, https://linkinghub.elsevier.com/retrieve/pii/S0017931007005108

ICCS Camera Ready Version 2023
To cite this paper please use the final published version:
DOI: 10.1007/978-3-031-36030-5_26